Sanchit Jain Rajan, Hari Krishna, Chikkadasappa Shivakumara, Madhu Gattumane Motappa, Bhangi Mutta Nagabhushana, Eco-friendly synthesis of biologically important $BiFeO_3$ and Ti^{4+}:$BiFeO_3$ for photocatalytic applications, Int.J.Curr.Biotechnol., 2015, 3(11):1-7.

International Journal of Current Biotechnology

ISSN: 2321 - 8371

Journal Homepage : http://ijcb.mainspringer.com

Eco-friendly synthesis of biologically important $BiFeO_3$ and Ti^{4+}:$BiFeO_3$ for photocatalytic applications

Sanchit Jain[1], Rajan Hari Krishna[1]*, Chikkadasappa Shivakumara[2], Madhu Gattumane Motappa[3], Bhangi Mutta Nagabhushana[1]

[1]Department of Chemistry, M. S. Ramaiah Institute of Technology, Bangalore 560 054, India.
[2]Solid State and Structural Chemistry Unit, Indian Institute of Science, Bangalore 560 012, India.
[3]Department of Chemical Engineering, M. S. Ramaiah Institute of Technology, Bangalore 560 054, India.

ARTICLE INFO

Article History:
Received 05 November 2015
Received in revised form 10 November 2015
Accepted 18 November 2015
Available online 20 November 2015

Key words:
Nano $BiFeO_3$, Solution combustion, Malachite green, Photocatalyst.

ABSTRACT

Metal ferrites are known to have excellent catalytic and antibacterial property. Synthesis of nano-ferrites is very significant in the development of novel functional materials for ecological and biological applications. We have synthesized biologically important $BiFeO_3$ and $BiFe_{0.95}Ti_{0.05}O_3$ through low temperature initiated solution combustion syntheses using urea as fuel. X-ray diffraction (XRD) and scanning electron microscopy (SEM) were used to examine the microstructure and morphology of the samples. X-ray peak broadening analysis showed that the crystallite sizes of the combustion derived products are in the range 25-30 nm. A comparative study on catalytic activities of the undoped and doped $BiFeO_3$ was carried out taking Malachite green (MG) as model pollutant. Catalysis efficiencies of the catalysts were tested under UV and visible light irradiation. The $BiFe_{0.95}Ti_{0.05}O_3$ sample exhibit better photocatalytic activity than undoped $BiFeO_3$. Further, the catalytic efficiency under visible light irradiation is found to be lesser than UV-light irradiation. The optimum catalyst dose was found to be 20 mg/L for 90% degradation of the dye, which is much lower than the reported catayst for MG degradation.

1. Introduction

With increasing revolution in science and technology, there was a bigger demand on opting for newer chemicals which could be used in various industrial processes. Among many new chemicals, organic dyes came up as one of the most widely used chemical stuff which could be used in many industrial activities. Due to the extensive use of these dyes in industries, they have become an integral part of industrial effluent. In fact, of the 450,000 ton of organic dyes annually produced worldwide, more than 11% is lost in effluents during manufacture and application processes (Forgas *et al*., 2004,). These organic dyes, typically azo dyes and fluorescein dyes have been reported to be highly cytotoxic for the mammalian tissues (Nony *et al*., 1980; Haveland-Smith *et al*., 1981). The organic groups present in dyes result in the formation of certain reactive intermediates, which trigger the morphological and genetic alterations, thereby making the dye cytotoxic and carcinogenic. Inoue *et al*., (2009) reported the carcinogenicity of anthraquinone dyes and found that the structure of the dye has an impact on the target organs. Therefore, disposal of the dyes from industrial wastewaters becomes a very relevant concern. But these dye molecules are normally difficult to be decomposed by natural means (Bhatnagar *et al*., 2005). Various methods, such as adsorption, advanced oxidation processes (AOPs), biological treatment, electrocatalysis and photocatalysis (Zhu *et al*., 2011; Anjaneya *et al*., 2011: Zhang *et al*., 2008; Bian *et al*., 2009), have been developed to remove organic dyes, in which the photocatalytic degradation of organic pollutants has received increasing interest owing to the absence of secondary pollution and the low cost by using solar light (Einaga *et al*., 2001).

Among all photocatalytic materials previously reported, TiO_2 is popularly regarded as the optimum photocatalyst for oxidative decomposition of organic compounds. Nevertheless, TiO_2 has a large band-gap of 3.2 eV and can only be excited by ultraviolet or near ultraviolet radiation, which accounts for only about 4% of the solar light spectrum (Anpo *et al*., 2003). In order to efficiently utilize the solar light in visible region (> 400 nm) for decomposition of organic compounds, development of visible light driven photocatalysts has attracted a tremendous amount of attention. To date, modifying TiO_2 and developing new photocatalytic materials are two general strategies to extend the response of a photocatalyst to the visible light range (Tang *et al*.,2004). Doping metals/nonmetals (Fuerte 2001: Zhao *et al*., 2002; Kato *et al*., 2002) and coupling with other lower band-gap semiconductors (Bessekhouad *et al*., 2005; Y.J. Yan

*Corresponding author.
Email address: rhk.chem@gmail.com
Mobile : 91 - 9886434109

et al., 2008) have been utilized to enhance the photocatalytic activity under visible light irradiation.

Perovskite-type samples having formula ABO_3 (A site is metal cation and B-site is transition metal) have been extensively studied as promising photocatalysts (Song *et al*.,2008). Among the different categories of photocatalysts, perovskite-type samples exhibit higher photocatalytic activity towards the degradation of organic compounds under visible light irradiation. Interestingly, it is also found to work steadily in various environments (Zhang *et al*.,2008). Because of the efficient photocatalytic behavior, a variety of methods, such as solid state reaction, sol-gel, hydrothermal technology, the polymerized complex technique and so on, have been applied to synthesize perovskite-type samples (Farhadi *et al*., 2009 ; Hosoya *et al*.,2005).

Malachite green (MG), tri-phenyl methane dye, has been widely used for the dyeing of leather, wool and silk as well as in distilleries (Cheng *et al*., 2008). In addition, MG also is used as a fungicide and antiseptic in aquaculture industry to control fish parasites and disease (Zhang *et al*., 2008). However, MG is very dangerous and highly cytotoxic to mammalian cells, and also acts as a liver tumor-enhancing agent. The dye blocks sunlight penetration upon been released into aquatic environment without degradation, thereby inhibiting the growth of aquatic plants and animals. (Bekci *et al*., 2009 ; Raghuvanshi *et al*., 2004). Therefore, there is considerable need to treat these effluents prior to their discharge into receiving waters to prevent environmental pollution in the aquatic ecosystems.

In the present investigation, $BiFeO_3$ and Ti: $BiFeO_3$ nanopowders were synthesized by low temperature solution combustion process and its application in the photocatalytic degradation of MG under UV and sunlight light is reported. The structure and morphology of prepared catalysts were characterized by X-ray diffraction (XRD), scanning electron microscopy (SEM) and UV-Vis spectroscopy. The probable reaction mechanism was proposed and discussed. The effects of various parameters such as catalyst dosage, and irradiation time on the photodegradation efficiency of MG were investigated.

2. Experimental

2.1 Chemicals

Bismuth nitrate ($Bi(NO_3)_3.4H_2O$), Ferric nitrate ($Fe(NO_3)_3$) and Urea ($CO(NH_2)_2$), were purchased from Merck. N-butyl titanate ($Ti(OC_4H_9)_4$) was purchased from Sigma Aldrich, Malachite green dye purchased from Nice chemicals and used without further purification.

2.2 Synthesis of undoped $BiFeO_3$

For the synthesis of $BiFeO_3$, stoichiometric amounts of Bismuth nitrate, Ferric nitrate are taken in a petri dish and required amount of Urea is subsequently added to the aqueous mixture of nitrates and continuously stirred, to ensure homogeneous mixing. The petri dish containing the homogeneous redox mixture is introduced into a muffle furnace maintained at 500±10 °C. Initially, the solution boils and undergoes dehydration. Eventually the mixture undergoes decomposition, which results in the liberation of large amounts of gases (usually CO_2, H_2O and N_2). This is followed by a spontaneous ignition which results in flame type combustion. The swelling of the reactant mixture is very typical of the flame type combustion. The process of converting aqueous mixture to a nano sized compound is over in less than 5 min and a highly porous $BiFeO_3$ is obtained, which is further grinded to get $BiFeO_3$ nanopowder.

2.3 Synthesis of Ti^{4+} doped $BiFeO_3$

Titanyl nitrate was prepared by taking N-butyl titanate in a petri dish and minimum quantity of water was added to hydrolyze butyl titanate to titanyl hydroxide. Further addition of HNO_3, titanyl nitrate was formed by the following reactions.

$$Ti(OC_4H_9)_4 + 3H_2O \longrightarrow TiO(OH)_2 + 4C_4H_9OH \quad \text{.....(1)}$$

$$TiO(OH)_2 + 2\,HNO_3 \longrightarrow TiO(NO_3)_2 + 2H_2O \quad \text{.....(2)}$$

The above titanyl nitrate was dissolved in minimum quantity water and added to the the stoichiometric quantities of Bismuth nitrate ($Bi(NO_3)_3.4H_2O$), Ferric nitrate ($Fe(NO_3)_3$) and Urea ($CO(NH_2)_2$), in the double distilled water and the further synthesis is similar to preparation of undoped $BiFeO_3$.

2.3. Characterization of photocatalyst

The phase purity and the crystallinity of the $BiFeO_3$ samples were examined by powder X-ray diffractometer (PANa-lytical X'Pert Pro) using CuKá (1.541 AU) radiation with a nickel filter running at 40 kV and 30 mA, scanning from 10° to 80° at 3°/min. The surface morphology of the product is examined by scanning electron microscopy (SEM) (JEOL JSM 840A). The FT-IR studies have been performed on a PerkinElmer Spectrometer (Spectrum 1000) with KBr pellets. The UV–vis absorption of the samples was recorded on SL 159 ELICO UV–VIS Spectrophotometer.

2.4. Photocatalytic activity test

The photocatalytic activity of synthesized $BiFeO_3$ and Ti^{4+}: $BiFeO_3$ were evaluated by the degradation of MG under UV and solar irradiation at room temperature. Prior to irradiation, the suspension containing MG and photocatalyst was magnetically stirred in dark for 1 h until the adsorption equilibrium was established. In all the experiments, 100 mL of dye solution of known concentration containing a known weight of Ti^{4+}:$BiFeO_3$/ $BiFeO_3$ powder was irradiated under the ultraviolet light lamp (15 W, ë=365 nm) maintaining the distance between the light source and the surface of the suspension about 10 cm. At regular time intervals, the suspension was taken out and centrifuged for 10 min to remove the catalyst particles completely. Further. the concentration of solution was analyzed by measuring the absorbance at ë max (664 nm) with a UV-Vis spectrophotometer.

The decolorization efficiency (%) was calculated as:

$$\text{Degradation (\%)} = (C0–C)/C0\times 100$$

Where C0 is the initial concentration of dye and C is the concentration of dye after photo irradiation.

3. Results and Discussion

3.1 Powder X-ray diffraction

In order to identify the phase and crystallographic purity of the synthesized final products, X-ray diffraction (XRD) was carried out. Fig. 1(a) is the XRD pattern of the undoped $BiFeO_3$, which matched well with the JCPDS Card No. 24-1422 of the $BiFeO_3$. Fig. 1(b) is the typical XRD pattern of the Ti^{4+} doped $BiFeO_3$. It can be seen clearly that all of the peaks can be indexed to the pure rhombohedral perovskite $BiFeO_3$ phase (according with JCPDS 86-1518). Moreover, it was also found that there are no impurity peaks corresponding to the dopent ions that show Ti^{4+} could be effectively built into the host

matrix. It is worth noticing that undoped sample consists of $Bi_{26}Fe_2O_{39}$ impurity peak (labelled as *) while in Ti^{4+} doped sample the impurity peak is not seen.

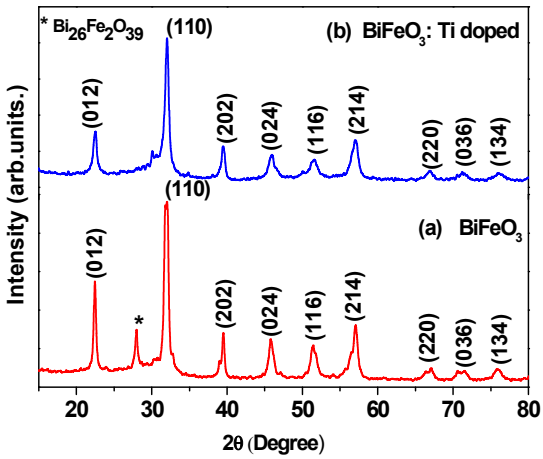

Figure – 1: PXRD patters of (a) Undoped $BiFeO_3$ (b) Ti: $BiFeO_3$

The average crystallite size estimated from the Debye–Scherrer's equation (Klug et al., 1954) is found to be in the range ~ 20-30 nm. Further, strain present in as-formed and calcined products was estimated using the W–H equation.(Williamson *et al*., 1953)

$$\beta\cos\theta = \frac{0.9}{\lambda} + 4\varepsilon\sin\theta \quad \ldots\ldots\ldots(3)$$

where ε is the strain associated with the nanoparticles. Equation (3) represents a straight line between 4 sinθ (X-axis) and β cosθ (Y-axis). The slope of line gives the strain (å) and intercepts (0.9ë/D) of this line on Y-axis gives grain size (D). Fig. 2 shows the W-H plots of undoped and Ti^{4+} doped $BiFeO_3$ samples. It is observed that the strain present in undoped sample is more when compared to doped $BiFeO_3$ samples, indicating that the reduction in the number of surface atoms with doping and reduction of surface defects. The estimated crystallite size values and strain values using Scherer's equation and W–H plots are given in Table 1.

Sample	Crystallite size (nm)		Strain X 10^{-4}
	Debye- Scherer	W-H method	
$BiFeO_3$	32.50	30.65	89.259
Ti:$BiFeO_3$	24	20	92.502

Table - 1: Crystallite size and lattice strain of $BiFeO_3$ and $BiFeO_3$:Ti^{4+}

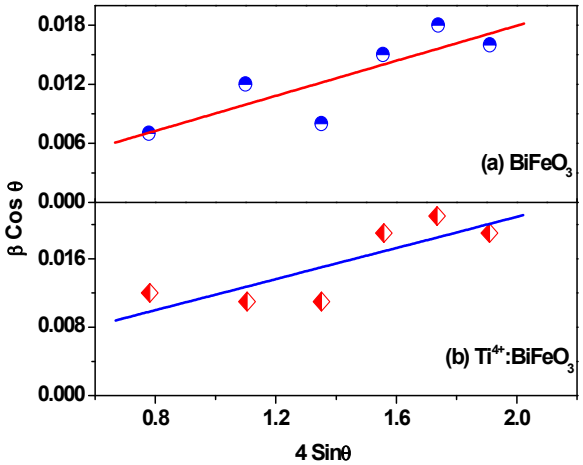

Figure – 2: Williamsom- Hall plot of (a) Undoped $BiFeO_3$ (b) Ti: $BiFeO_3$

3.2 Fourier Transform Infra red spectroscopy

Figure 3(a) and 3(b) shows the FTIR spectra of undoped and Ti^{4+} doped $BiFeO_3$. The fundamental absorptions are observed at 433 and 526 cm^{-1}, these are due to bending and stretching vibrations of Fe-O bond respectively in the FeO_6 octahedral unit (Rao *et al*., 1970 ; Som *et al*., 1992). A prominent band at ~815 cm^{-1} is evident for the presence of carbonate groups, that are formed during combustion from the fuel used as precursor (Zhang *et al*., 2006). No significant shift is observed in peaks due to Ti^{4+} doping.

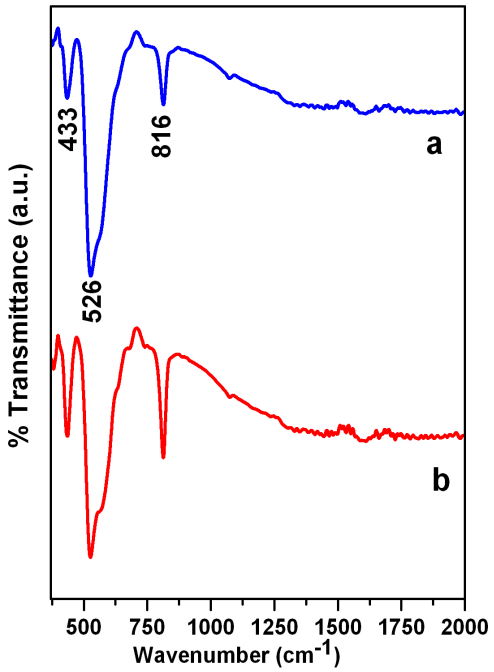

Figure – 3: FTIR spectra of (a) undoped $BiFeO_3$ (b) Ti: $BiFeO_3$

3.3 Scanning Electron Microscopy

Fig. 4a and 4b shows typical electron micrographs of the combustion derived $BiFeO_3$ and Ti^{4+} doped $BiFeO_3$ catalysts respectively. It can be seen in the SEM images that the porosity increases with addition of Ti^{4+}. It is well known that, combustion synthesis reaction is influenced by metal–ligand complex formation between metal ion of oxidizer and fuel. Depending upon the type of fuel used and type of metal involved, the nature of combustion differs from flaming (gas phase) to non-flaming (smouldering and heterogeneous) type. Generally, flaming reactions involve liberation of a large quantity of gases. Interestingly, it was observed during combustion reaction that the moderately flame type combustion turns to more vigorous flaming type with the addition of Ti^{4+}. In a typical combustion reaction, the Ti^{4+} is expected to form a uniform complex with the urea ligand, more easily than Fe^{3+} because of high positive charge on Ti^{4+}. Therefore, an increase in the porosity of the samples with the addition of Ti^{4+} can be assumed to be due to uniformity in the distribution of urea which leads to liberation of large quantities of gas evenly.

3.4 UV-Visible

The UV-Vis spectra were recorded in the wavelength region of 200-700 nm for undoped and Ti^{4+} doped $BiFeO_3$ are shown in Fig. 5 (a) and (b) respectively. In Ti^{4+}-doped sample, sharp absorption peaks at ~256 and 340 nm, along with broad absorption at ~460 nm are observed. However, in undoped sample, broad absorption peaks at ~250-350 nm were observed. In addition to these peaks broader absorption ranging from 400-600 nm is also seen in undoped $BiFeO_3$. These indicate a change in the electronic structure of $BiFeO_3$ with Ti^{4+} doping. It is

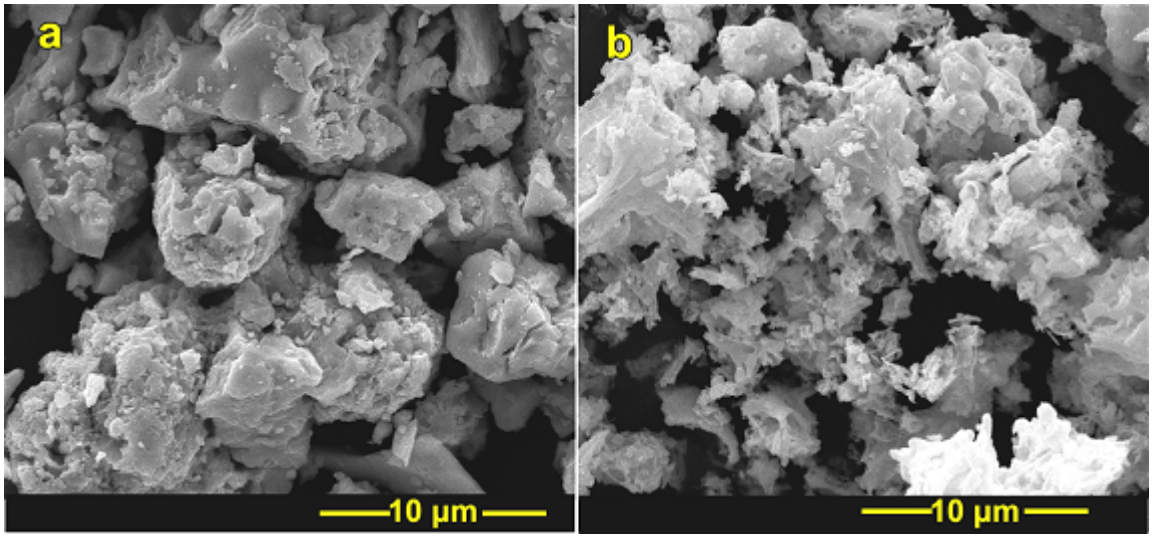

Figure – 4: Scanning electron micrographs of (a) Undoped $BiFeO_3$ (b) Ti: $BiFeO_3$

interesting to note with Ti^{4+} doping a significant shift of absorption peaks towards the shorter wavelength side is observed, which might be due to the creation of oxygen vacancy (Roy *et al*., 2007). These indicate an obvious blue shift when $BiFeO_3$ is doped with titanium and might influence the band structure of the material. Change in band structure with doping is also reported by Mukherjee et.al for yttrium doped bismuth ferrite nanoparticles synthesized by modified Pechini technique (Mukherjee *et al*., 2012).

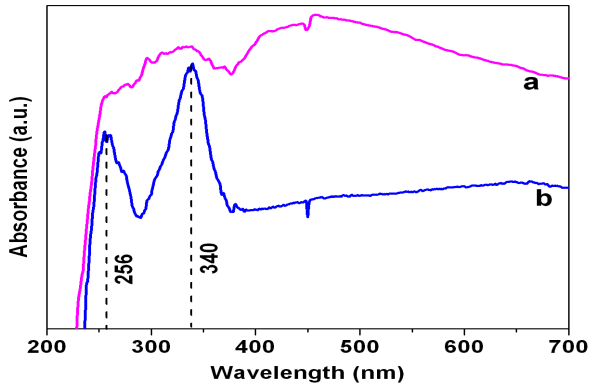

Figure – 5: UV-Visible absorption spectra of (a) Undoped $BiFeO_3$ (b) Ti: $BiFeO_3$

4. Photocatalytic activity of $BiFeO_3$ nanopowder

4.1 *Photocatalytic performance of $BiFeO_3$ and Ti^{4+} doped $BiFeO_3$ on different conditions*

To evaluate the photocatalytic activity of the undoped and Ti^{4+} doped $BiFeO_3$, experimental runs using solutions of the MG dye as a model substance were carried out at different treatment processes such as: Undoped $BiFeO_3$ for photocatalytic activity under Sunlight and UV light with variable parameters. Similarly Ti^{4+} doped $BiFeO_3$ as photocatalyst under sunlight and UV light irradiation are investigated.

4.2. Effect of catalyst loading

The effect of catalytic loading on degradation of MG dye over $BiFeO_3$ and Ti:$BiFeO_3$ under Visible light irradiation is shown in Fig.6 a and Fig.6 b respectively. The figures show that % degradation of MG was maximum when the amount of catalyst was 2 mg/100 ml. It should be pointed out that, the catalyst loading affects number of active sites on the photocatalyst and the penetration of radiation through the suspension. As the catalyst loading increases the % removal of MG decreases due to the enhancement of light reflectance by catalyst particles. The number of active sites increases but the penetration of radiation decreases due to shielding effect (Goncalves *et al*., 1999). Photocatalytic degradation rate, which is influenced by both the number of active sites and the penetration of irradiation light, must therefore pass through a maximum at optimum catalyst loading. Also, the decrease in adsorption density with increase in adsorbent amount is due to the high number of unsaturated adsorption sites (Salim *et al*., 2002). It should also be noted that the optimum value of catalyst loading is strongly dependent on the type and initial concentration of the pollutant and the operating conditions of the photoreactor (Gogate *et al*., 2004). In our study, the optimum catalyst loading for $BiFeO_3$ and Ti:$BiFeO_3$ are found to be 20 mg/L

4.3. Effect of stirring time

The photo assisted decolorization of MG was also carried out using optimum amount of $BiFeO_3$ and Ti: $BiFeO_3$ with optimum catalyst loading under solar and UV irradiation. Fig. 7 depicts the results of photodecolorization of MG dye using optimized conditions as a function of stirring time under solar light and UV light using doped and undoped $BiFeO_3$. It is clear from the degradation plot that the decolorization of MG was faster and more effective for Ti: $BiFeO_3$ under both sunlight and UV light irradiation. When Ti: $BiFeO_3$ was used the percentage degradation of MG was 90 and 60% under UV light and sunlight respectively, whereas for undoped $BiFeO_3$ the percentage degradation of MG is 70 and 40% under UV and sunlight respectively.

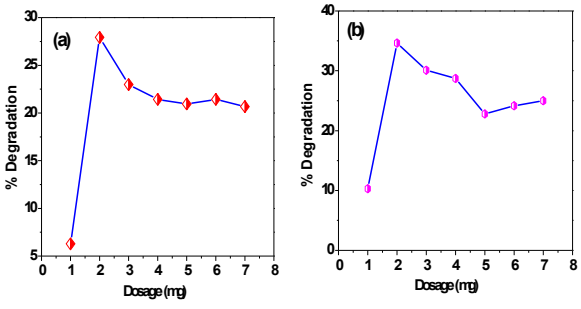

Figure – 6: Plot of percentage degradation vs. catalyst dose (initial dye concentration: 5 mg/L, irradiation time: 30 min) for $BiFeO_3$ (a) Under sunlight (b) under UV light

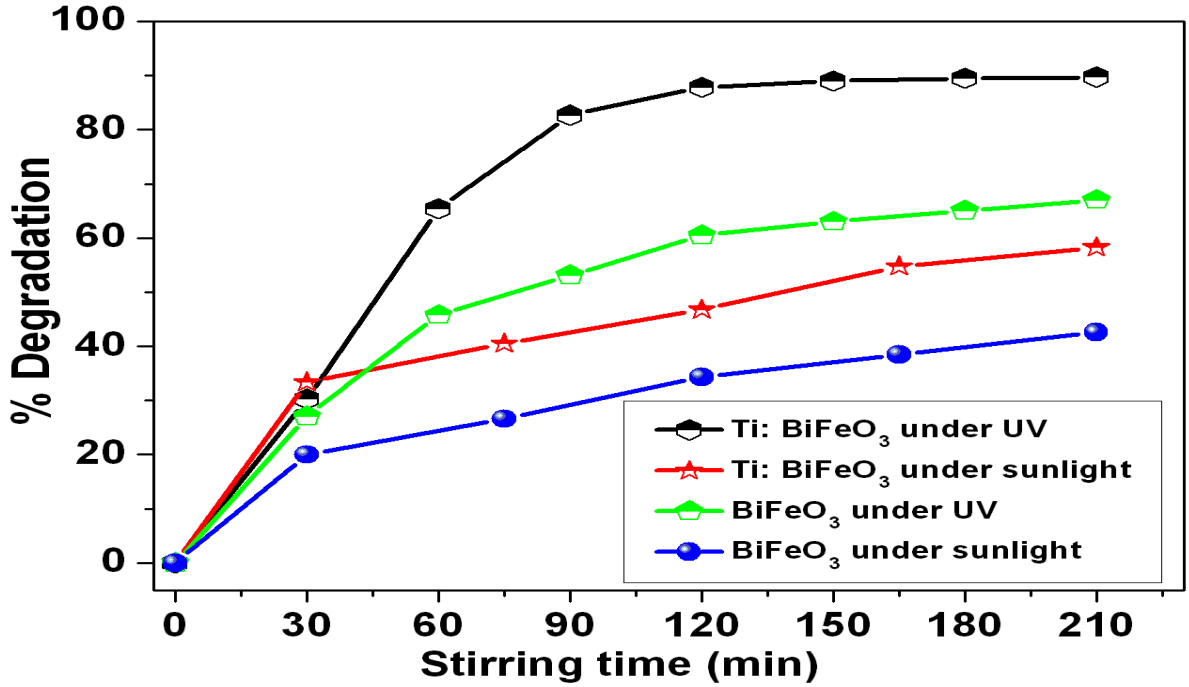

Figure – 7: Plot of percentage degradation vs. irradiation time for $BiFeO_3$ and $Ti:BiFeO_3$ under different light sources

4.3. Photocatalytic kinetics

The photocatalytic kinetics of the $BiFeO_3$ and $BiFeO_3$:Ti^{4+} nanoparticles under UV light and sunlight were also investigated. Langmuir–Hinshelwood model expressed in Eq. (4) was applied to understand the reaction kinetics quantitatively. This model has been used to calculate the rate constant of photocatalytic experiments (Xiong Wang *et al*., 2011).

$$r = -\frac{dc}{dt} = \frac{k_r KC}{(1 + KC)} \quad \ldots\ldots\ldots\ldots (4)$$

where r is the reaction rate, k_r is the reaction rate constant, K is the absorption coefficient of the reactant, and C is the reactant concentration. When C is very small, Eq. (4) can be expressed by Eq. (5).

$$r = -\frac{dc}{dt} = k_r KC = kC \quad \ldots\ldots\ldots\ldots (5)$$

where k is the first-order rate constant. Set t=0, $C = C_0$, Eq. (6) can be induced.

$$\ln \frac{C_o}{C} = kt \quad \ldots\ldots\ldots\ldots (6)$$

Fig. 8(a) and (b) shows the photocatalytic activities of $BiFeO_3$ under sunlight and UV light respectively. It is clear that the kinetic simulation curve with irradiation time (t) as abscissa and $\ln(C_0/C)$ as the vertical ordinate is close to a linear curve with the fitting constant R greater than 0.96. It is observed that $BiFeO_3$:Ti^{4+} exhibit enhanced photocatalytic activity ($k = 0.0180\ min^{-1}$) under UV light and the least photocatalytic activity was shown by undoped $BiFeO_3$ under sunlight ($k = 0.0033\ min^{-1}$). Details of fitting constant (R^2) and k values obtained are summarized in Table. 2

Sample	Under UV light		Under sunlight	
	R^2	$k\ (min^{-1})$	R^2	$k\ (min^{-1})$
$BiFeO_3$	0.96	0.0084	0.95	0.0033
$BiFeO_3$: Ti^{4+}	0.98	0.0180	0.95	0.0050

Table - 2: Reaction kinetic parameters obtained for $BiFeO_3$ and $BiFeO_3$: Ti^{4+}

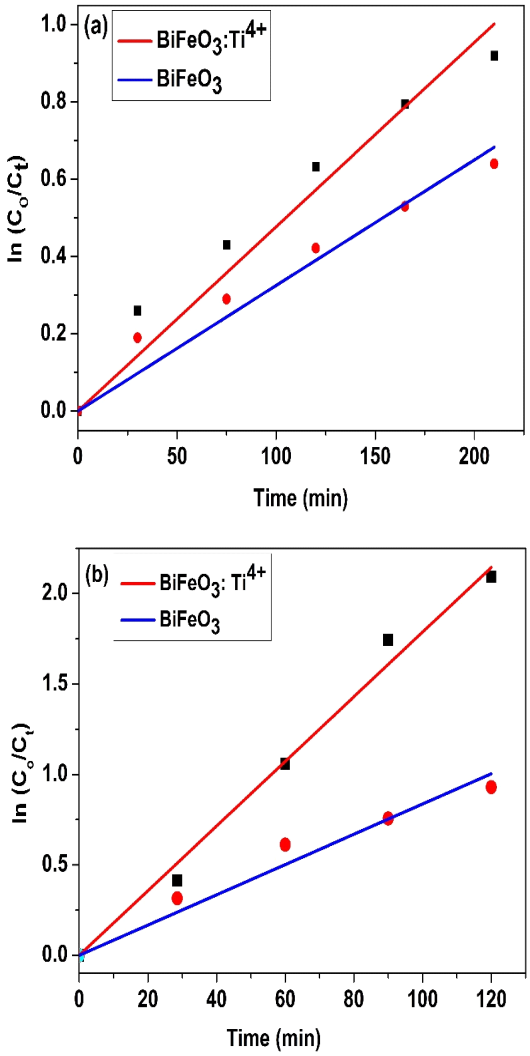

Figure – 8: Photocatalytic kinetics of $BiFeO_3$ nanoparticles under (a) Sunlight (b) UV light

4.4 Mechanism of Catalysis

The Electronic band structure of $BiFeO_3$ (Fig.9) consists of conduction band of Fe 3d states and valence band of O 2P states and the electronic transitions involved are the charge transfer transitions from O:2p → Fe:3d which could be a combination of LMCT (Ligand to Metal Charge Transfer) and MMCT (Metal to Metal charge transfer) (Clarck *et al.,* 2007). When light interacts with $BiFeO_3$ electrons in valence band get promoted to conduction band that creates positively charged holes in the valence band. Hydroxyl radicals are produced due to positive potential of the valence band on the other hand O_2 is reduced due to negative potential of the conduction band. The hydroxyl radical (or hole) is a powerful oxidizing agent and readily degrades the organic pollutants in the vicinity of the catalyst surface. When Ti^{4+} is doped into $BiFeO_3$, Ti^{4+} gets substituted at the Fe^{3+} sites, thus it creates imbalance in charge when +3 ion is replaced with +4 ion. To maintain charge state of metal ions intermediate energy levels or surface states are created within the band gap of the material, this increases the probability of the charge carriers reacting at the surface due to reduced diffusion lengths. This might be the reason for increased photocatalytic activity of Ti^{4+} doped material when compared to undoped $BiFeO_3$.

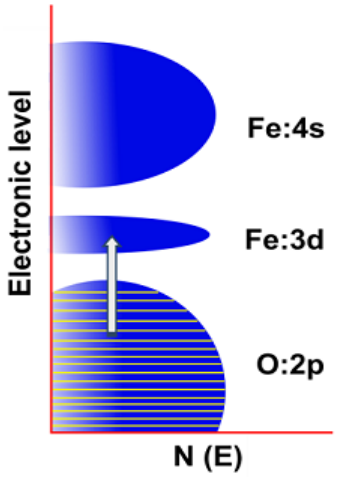

Figure – 9: Band structure of $BiFeO_3$ (↑ indicate charge transfer)

The significance of the present study is that in addition to available methods of improving catalytic efficiency, doping mechanism could greatly contribute to the improvement of photocatalytic property. The current results show that little chemical manipulation like Ti^{4+} doping can create favorable electronic energy scheme that results in favorable electronic band structure contributing to higher photocatalytic activity. Another important contribution of this work is doping $BiFeO_3$ with significantly less amount of Ti^{4+} greatly reduces the catalyst loading for optimum efficiency making photocatalytic process cost effective (20 mg/L). This raises hope for future work on doped $BiFeO_3$ for even better performance, as the separation efficiency of electron-hole pair could be higher and recombination of charge carriers could be significantly reduced.

Conclusions

Undoped and Ti^{4+} doped $BiFeO_3$ samples were successfully prepared by low temperature solution combustion method and characterized for its application in photo catalytic degradation of MG dye. PXRD results showed that Ti^{4+} could be effectively incorporated into the $BiFeO_3$ crystal lattice and theoretical crystallite size calculated from X-ray line broadening were in the range ~30 nm and ~18 nm for $BiFeO_3$ and Ti:$BiFeO_3$ samples respectively. Scanning electron micrographs shows that more porous structure with large voids for Ti:$BiFeO_3$ sample compared to undoped $BiFeO_3$. UV-Visible absorbance spectra shows Ti:$BiFeO_3$ has favorable absorbing range that makes it better photocatalyst than undoped one. Accordingly $BiFeO_3$ showed photocatalytic activity under UV and sunlight that further greatly enhanced with Ti^{4+} doping. Mechanism for the observed photocatalysis is proposed and optimum conditions for better catalytic activity were explored.

References

Anjaneya, S.Y. Souche, M. Santoshkumar, T.B. Karegoudar, Decolorization of sulfonated azo dye Metanil Yellow by newly isolated bacterial strains: Bacillus sp. strain AK1 and Lysinibacillus sp. strain AK2, J Hazar. Mat. 190 351-358 (2011).

Anpo, M. Takeuchi, The design and development of highly reactive titanium oxide photocatalysts operating under visible light irradiation, *J. Catal.* 216, 505–516 (2003).

Bessekhouad, D. Robert, J.V. Weber, Photocatalytic activity of Cu_2O/TiO_2, Bi_2O_3/TiO_2 and $ZnMn_2O4/TiO_2$ heterojunctions , *Catal. Today* 101, 315–321 (2005).

Bekci, Y. Seki, L. Cavas, Removal of malachite green by using an invasive marine alga Caulerpa racemosa var. cylindracea, *J. Hazard. Mater.* 161, 1454–1460 (2009).

Bhatnagar, A.K. Jain, A comparative adsorption study with different industrial wastes as adsorbents for the removal of cationic dyes from water, J. Colloid Interface Sci. 281, 49–55, (2005).

Bian, Y.N. Huo, Y. Zhang, J. Zhu, Y.F. Lu, H.X. Li, Aerosol-spay assisted assembly of $Bi_2Ti_2O_7$ crystals in uniform porous microspheres with enhanced photocatalytic activity, App. Catalysis B, 91, 247-253 (2009).

Cheng, S.-G. Wang, L. Lu, W.-X. Gong, X.-W. Liu, B.-Y. Gao, H.-Y. Zhang, Removal of malachite green (MG) from aqueous solutions by native and heat-treated anaerobic granular sludge, *Biochem. Eng. J.* 39, 538–546 (2008).

Clarck, Robertson, Band gap and Schottky barrier heights of multiferroic $BiFeO_3$, *J App. Phys. Lett.,* 80, 132903-132906 (2007).

Einaga, S. Futamura, T. Ibusuki, Complete oxidation of benzene in gas phase by platinized titania photocatalysts, *Environ. Sci. Tech.* 35, 1880-1884 (2001).

Farhadi, Z. Momeni, M. Taherimehr, Rapid synthesis of perovskite-type $LaFeO_3$ nanoparticles by microwave-assisted decomposition of bimetallic $La[Fe(CN)_6]\cdot 5H_2O$ compound, *J. Alloy. Compd,* 471, L5–L8 (2009).

Forgas, T. Cserhati, G. Oros, Removal of synthetic dyes from wastewater: a review, Environ. Inter. 30, 953–971 (2004).

Fuerte, M.D. Hernández-Alonso, A.J. Maira, A. Martinez-Arias, M. Fernandez-Garcia, J.C. Coneasa, J. Soria, Visible light-activated nanosized doped-TiO_2 photocatalysts, *Chem. Commun.* 40, 2718–2719 (2001).

Gogate, A.B. Pandit, A review of imperative technologies for wastewater treatment: oxidation technologies at ambient conditions, *Adv. Environ. Res.,* 8, 501-551 (2004).

Goncalves, A.M.F. Oliveira-Compos, E.M.M.S. Pinto, P.M.S. Plasencia, M.J.R.P. Queiroz, Photochemical treatment of solutions of azo dyes containing TiO_2 *Chemosphere* 39, 781-786 (1999).

Haveland-Smith, R.D. Combes, B.A. Briges, Studies on the genotoxicity of some fluorescein dyes, Mutation Research, 88, 1-15 (1981).

Hosoya, Y. Itagaki, H. Aono, Ozone detection in air using $SmFeO_3$ gas sensor, *Sensor. Actuat. B-chem* 108, 198–201 (2005).

Inoue, M. Yoshida, M. Takahashi, H. Fujimoto, K. Ohnishi, K. Nakashima, M. Shibutani, M. Hirise, A. Nishikawa, Possible contribution of rubiadin, a metabolite of madder color, to renal carcinogenesis in rats, Food Chem. Toxicol. 47, 752–759 (2009).

Kato, A. Kudo, Visible-light-response and photocatalytic activities of TiO_2 and $SrTiO_3$ photocatalysts codoped with antimony and chromium, *J. Phys. Chem. B* 106, 5029–5034 (2002).

Klug, L.E Alexander, *X-Ray Diffraction Procedure*, Wiley, New York, 1954.

Mukherjee, Sk. M. Hossain, M. Pal, S. Basu, Effect of Y-doping on optical properties of multiferroics $BiFeO_3$ nanoparticles, Appl Nanosci. 2, 305–310 (2012).

Nony, M.C. Bowman, T. Cairns, Metabolism studies of an azo dye and pigment in the hamster based on analysis of the urine for potentially carcinogenic aromatic amine metabolites, J. Anal. Toxicol. 4, 132-140 (1980).

Raghuvanshi, R. Singh, C.P. Kaushik, Kinetics study of methylene blue dye bioadsorption on baggase, *Appl. Ecol. Environ. Res.* 2, 35–43 (2004).

Rao, CNR. Rao, Infrared and electronic spectra of rare earth perovskites: ortho-chromites, -manganites and –ferrites, Appl Spectrosc 24, 436–445 (1970).

Roy, GL. Sharma, MC .Bhatnagar. Large blue shift in the optical band-gap of sol–gel derived $Ba_{0.5}Sr_{0.5}TiO_3$ thin films, *Solid State Commun* 141(5), 243-247 (2007).

Salim, F. Othman, M.d. Imtiaj Ali, J. Patterson, T. Hardy, Application of locally available materials for the treatment of organic polluted water, *Water Sci. Technol*. 46, 339–346 (2002).

Som, S. Molla, K. Bose, BK. Chaudhury, Nonlinear physical properties of amorphous $Bi_4Sr_3Ca_3CuyOx$ semiconducting oxides with y between 0 and 5, *Phys Rev B.* 45(4) 1655–1659 (1992).

Song, L.J. Xu, Z.Q. He, H.P. Ying, J.M. Chen, Photocatalytic degradation of C.I. Direct Red 23 in aqueous solutions under UV irradiation using $SrTiO_3$/CeO_2 composite as the catalyst, *J. Hazard. Mater* 152, 1301–1308 (2008).

Tang, Z.G. Zou, J.H. Ye, Efficient Photocatalytic Decomposition of Organic Contaminants over $CaBi_2O_4$ under Visible-Light Irradiation *, Angew. Chem. Int.Ed.* 43, 4463–4466 (2004).

Williamson, W.H. Hall, X-ray line broadening from filed Aluminium and Wolframe, *Acta Metall*. 1, 22-31(1953).

Xiong Wang, Ying Lin, Xifeng Ding, Jinguo Jiang, Enhanced visible-light-response photocatalytic activity of bismuth ferrite nanoparticles, *J. Alloy. Compd,* 509, 6585–6588 (2011).

Yan, X.Q. Qiu, H. Wang, L.P. Li, X.Z. Fu, L. Wu, G.S. Li, Synthesis of ZnO/titanate nanocomposites with highly photocatalytic activity under visible light irradiation, *J. Alloy Compd*. 460, 491–495 (2008).

Zhang, LH. Pang, Y. Zhang, Lu MH, YF .Chen, Preparation, structures, and multiferroic properties of single phase $Bi_{1-x}La_xFeO_3$ (x=0–0.40) ceramics *, J Appl Phys.* 100(11), 114108-114108-6 (2006).

Zhang, F.L. Yang, M.M. Gao, L.F. Liu, Electrocatalytic Behavior of the Bare and the Anthra quinone disulfonate/ Polypyrrole Composite Film Modified Graphite Cathodes in the Electro-Fenton System, J Phys.Chem. C 112, 8957-8962 (2008).

Zhang, X.Y. Fu, S.Y. Niu, Q. Xin, Synthesis and photoluminescence properties of Eu^{3+}-doped $AZrO_3$ (A = Ca, Sr, Ba) perovskite, *J. Alloy. Compd* 459, 103–106 (2008).

Zhang, Y. Li, C. Zhang, Y. Jing, Adsorption of malachite green from aqueous solution onto carbon prepared from Arundo donax root, *J. Hazard. Mater*. 150, 774–782 (2008).

Zhao, C.C. Chen, X.Z. Li, J.C. Zhao, H. Hidaka, N. Serpone, Photodegradation of sulforhodamine-B dye in platinized titania dispersions under visible light irradiation: influence of platinum as a functional co-catalyst, *J. Phys. Chem*. B 106 5022–5028 (2002).

Zhu, S.L. Wang, S.H. Xie, H.X. Li, Hexagonal single crystal growth of WO_3 nanorods along a [110] axis with enhanced adsorption capacity , Chem. Comm. 47, 4403-4405 (2011).
